Asia-Pacific J. Atmos. Sci., 48(3), 213-226, 2012
DOI:10.1007/s13143-012-0022-6

Changes in Climate Classification and Extreme Climate Indices from a High-Resolution Future Projection in Korea

Kyung-Sook Yun[1], Ki-Young Heo[1,2], Jung-Eun Chu[1], Kyung-Ja Ha[1], Eun-Jeong Lee[1], Yumi Choi[1], and Akio Kitoh[3]

[1]*Division of Earth Environmental System, College of Natural Science, Pusan National University, Busan, Korea*
[2]*Coastal Disaster Research Center, Korea Institute of Ocean Science and Technology, Ansan, Korea*
[3]*Meteorological Research Institute, Tsukuba, Ibaraki, Japan*

(Manuscript received 28 December 2011; revised 13 February 2012; accepted 19 February 2012)

Abstract: We investigate the future changes in the climate zone and six extreme temperature indices in Korea, using the 20-km high-resolution atmospheric general circulation model (MRI-AGCM3.1S). The Trewartha and Köppen climate classification schemes are applied, and four summer-based extreme temperature indices (i.e., summer days, tropical nights, growing degree days, and cooling degree days (CDD) and two winter-based indices (frost days and heating degree days (HDD) are analyzed. To represent significantly the change in threshold indices, the monthly mean bias is corrected in model. The model result reasonably captures the temporal and spatial distribution of the present-day extreme temperatures associated with topography. It was found that in the future climate, the area of the subtropical climate zone in Korea expands northward and increases by 21% under the Trewartha classification scheme and by 35% under the Köppen classification scheme. The spatial change in extreme climate indices is significantly modulated by geographical characteristics in relation to land-ocean thermal inertia and topographical effects. The change is manifested more in coastal regions than in inland regions, except for that in summer days and HDD. Regions with higher indices in the present climate tend to reveal a larger increase in the future climate. The summer-based indices display an increasing trend, while the winter-based indices show a decreasing trend. The most significant increase is in tropical nights (+452%), whereas the most significant decrease is in HDD (-25%). As an important indicator of energy-saving applications, the changes in HDD and CDD are compared in terms of the frequency and intensity. The future changes in CDD reveal a higher frequency but a lower temperature than those in HDD. The more frequent changes in CDD may be due to a higher and less dispersed occurrence probability of extreme temperatures during the warm season. The greater increase in extreme temperature events during the summer season remains an important implication of projecting future changes in extreme climate events.

Key words: Extreme climate, future climate change, East Asian climate, high resolution model, climate classification

1. Introduction

The assessment of global climate change due to increases in greenhouse gas concentrations is one of the major issues of current climate research. The most important point in the climate change is the increase in unprecedented extreme climate events, because of their extensive effects on diverse fields such as agriculture, public work, and water resources. Significant changes in climate extremes have already been observed across the Asia-Pacific region during the past few decades (Zhai *et al*., 2005; Alexander *et al.*, 2006). Meehl *et al*. (2000) have reported that a small increase in the mean temperature can induce drastic changes in extreme climates. This implies that changes in extreme climate events such as floods, heat waves, and cold surges are much more conclusive than the changes determined from seasonal mean states. In particular, changes in extreme climate are not uniform in time and space. For these reasons, many previous studies have focused on regional climate changes in the extreme temperature and precipitation (Bonsal *et al.*, 2001; Alexander and Arblaster, 2008; Yun *et al.*, 2008; Jung *et al.*, 2011). In this study, our main concern is the regional climate change in extreme temperature events, focusing on Korea.

Recently, regional climate change over East Asia, particularly Korea, has been examined in many studies using observational and model simulation datasets. These results exhibit a coherent change in extreme climate events throughout Korea. In particular, there is an increase in warm extreme events and decrease in cold extreme events, owing to the warmer climate. Boo *et al*. (2006) have shown that an increase in mean temperature produces an increase in the frequency and intensity of extreme rainfall. Im *et al*. (2011) have evaluated future trends in extreme temperature and rainfall indices over Korea. It was reported that changes in all the extreme indices is rapidly accelerated in the future climate, and this is particularly evident in the indices based on daily maximum temperature (Tmax). In addition, to reduce the uncertainty in regional extreme climates, Ho *et al.* (2011) have shown the changes of extreme climate events in various emission scenarios over Korea. The future changes predicted for heat waves are largest, with projected increasing ranging from 294% to 583%, depending on the prescribed emission profile.

Many efforts have been made to advance knowledge of climate change indices, primarily focusing on climate extremes.

Corresponding Author: Kyung-Ja Ha, Department of Atmospheric Sciences, Pusan National University, Busandaehak-ro 63beon-gil, Geumjeong-gu, Busan 609-735, Korea.
E-mail: kjha@pusan.ac.kr

The joint World Meteorological Organization (WMO) Commission for Climatology (CCl)/World Climate Research Programme (WCRP) project on Climate Variability and Predictability (CLIVAR)/Joint WMO-IOC Technical Commission for Oceanography and Marine Meteorology (JCOMM) Expert Team on Climate Change Detection and Indices (ETCCDI) has recommended a vast range of possible indices. The indices can largely be categorized into 5 different groups: percentile-based indices (e.g., occurrence of cold nights; TN10p), absolute indices (e.g., maximum daily minimum temperature (Tmim)), threshold indices (e.g., number of heavy precipitation days > 10 mm), duration indices (e.g., cold spell duration indicator), and other indices that include diurnal temperature range (Alexander *et al.*, 2006). Distribution parameters of these indices include their frequency, intensity, and shape clustering in space or time. The Fourth Assessment Report of the Intergovernmental Panel on Climate Change (IPCC AR4) has reported that the increase in frequency of extreme climate events is consistent with the increases in greenhouse gas concentrations (Trenberth *et al.*, 2007), implying the significant impact of global warming on extreme climate events. As the series of an effort to understand the extreme climate change, the Special Report on "Managing the Risks of Extreme Events and Disaster to Advance Climate Change Adaptation" (SREX) Summary for Policymakers (SPM) is now open, although the full report will be published in February 2012.

Although future changes in extreme climate indices have been investigated in many studies, detailed spatial change in the daily extreme indices, focusing on Korea, has not yet been explicitly examined. Owing to the significant uncertainty in climate simulations, it is necessary to quantify future changes of extreme frequency and intensity using more varied approaches and a high-resolution model. In particular, the East Asian climate is modulated by a complex feedback mechanism and multi-scale interactions from meso-scale to planetary scale. Because of the significant difference between the climate extremes in low and high resolution models, the need for high resolution modeling has been suggested in previous studies (Feng *et al*., 2011; Li *et al*., 2011a, 2011b). Therefore, to investigate the regional climate change in extremes, we use 20-km mesh atmospheric general circulation model (AGCM). This high-resolution model may provide reliable simulations in terms of topography-related weather and climate events.

In the present study, we analyze changes in extreme temperature indices because studies on comparison of observed and modelled trends in climate temperature and precipitation extremes reveal reasonably good agreement only with temperature trends (e.g., Kharin *et al*., 2007; Kiktev *et al*., 2007). To investigate future changes in extreme temperature indices, we have mainly used threshold indices such as the annual number of summer days (SD), tropical nights (TN), and frost days (FD). In addition, to provide special information for agricultural and energy-saving applications, the changes in growing degree days (GDD), heating degree days (HDD), and cooling degree days (CDD) are analyzed. Meanwhile, the change in climate classification (particularly the subtropical climate zone) has important implications for the extreme climate events. Because the subtropical climate zone is characterized by hot, humid summers and no specific dry season. This climate condition provides a potential possibility to appear more intense, more frequent, and longer lasting extreme climate events including heavy rainfall and heat waves, due to a warmer temperature and increased convection and evaporation. Despite their importance, future changes in climate classifications over Korea have not yet been firmly demonstrated in previous studies. Several studies have examined only changes in the subtropical climate zone (e.g., Kwon *et al.*, 2007). Therefore, we investigate future changes in the subtropical climate zone, as well as changes in extreme climate events. In summary, we examine the present characteristics of extreme temperatures (i.e., Tmax and Tmin) and validate the model result in comparison with the observations. On the basis of these results, future changes in the subtropical climate zone and in extreme temperature indices are quantitatively investigated in time and space.

2. Model and indices

a. Model and data

The 20-km high-resolution AGCM (MRI-AGCM3.1S) is used to describe the detailed regional future changes in climate classification and extreme climate events over the East Asian region especially over Korean Peninsula. This high-resolution AGCM was jointly developed by the Japan Meteorological Agency (JMA) and the Meteorological Research Institute (MRI).

The resolution of the model is triangular truncation 959 with the linear Gaussian grid, which corresponds horizontally to a 20 km-mesh, and vertically to 60 layers with the model top at 0.1 hPa. For this time-slice, climate simulations were carried out for three different periods. The first, present-day was simulated for 25 years (1979-2003), using observed sea surface temperatures (SST) and sea-ice concentrations. For the future climate, two time-slice 25-year simulations corresponding to the near future (2015-2039) and the end of 21st century (2075-2099) were performed. Hereafter, the present, near future, and future climate are referred to as the periods 1979-2003, 2015-2039 and 2075-2099, respectively. Future changes in SST were evaluated as the difference between the 20th century simulation and future simulations by the 18 atmosphere-ocean coupled general circulation models for the 3rd phase of the Coupled Modeling Intercomparison Project (CMIP3) under the Special Report on Emission Scenarios (SRES) A1B emission scenario. The design retains observed year-to-year variability and El Nino and Southern Oscillation (ENSO) events in the future climate, but with a higher mean and clear increasing trend in SST. Future sea-ice distribution is obtained in a similar fashion. Details of the method are described in Mizuta *et al.* (2008). Kitoh and Kusunoki (2008) have reported that due to its high horizontal resolution, the 20-km mesh AGCM captures

orographic rainfall well, not only in terms of its location, but also in terms of its amount. The use of high-resolution topography may contribute to the realistic simulation of extreme temperature indices.

To validate model reliability, Korean Meteorological Administration (KMA) synoptic station data from 76 stations are used. The extreme temperatures (i.e., daily Tmax and Tmin) are compared with the simulated results in the present climate. The period used is from 1979 to 2003, corresponding to the present climate period. The observational dataset exhibits a significant performance of the 20-km high- resolution model in terms of the annual cycle and spatial structure.

b. Subtropical climate zone

To define the subtropical climate zone, we applied two climate classification schemes: Trewartha (1968) and Köppen (1918). Trewartha (1968) has identified the subtropical climate zone using only monthly mean temperature (Tave). Due to the simple calculation process, the Trewartha scheme has been widely used to classify this climate region (e.g., Kwon *et al*., 2007). The subtropical climate zone is defined as the region where the temperature of the coldest month is less than or equal to 18°C and the temperature is greater than or equal to 10°C for more than 8 months. To classify the climate region in more detail, Köppen (1918) considers monthly mean precipitation as well as monthly Tave. World climate is divided into five main groups. Korea is geographically situated on a mixed region than incorporates temperate/mesothermal climate (C) and continental/microthermal climate (D). D climate is defined as a region where the temperature of the coldest month is below −3°C and the temperature of the warmest month is above 10°C. Meanwhile, C climate is identified as a region where the temperature of the coldest month is above −3°C and below 18°C. Sort a indicates a region where Tave of the warmest month is greater than or equal to 22°C, while b indicates the opposite region to a. According to precipitation, dryness in the winter (w) and wetness in all season (f) are divided in terms of the precipitation of the wettest month and the driest month during summer and winter, respectively. The details are represented in Table 1. In the present study, the subtropical climate region of Köppen scheme is suggested as both Cwa and Cfa. Although the Köppen classification scheme does not classify exactly the subtropical climate, C climate generally has warm and humid summers. In particular, Cwa and Cfa are referred as the humid subtropical climate (e.g., Rolim *et al*., 2007). Finally, the subtropical climate zones are calculated for the 25-yr climatology (e.g., 1979 to 2003 in the present climate).

c. Extreme climate indices

Daily Tmax and Tmin are used to extract a total of 6 extreme climate indices including SD, TN, FD, GDD, HDD, and CDD. These extreme temperature indices are defined by a fixed threshold of extreme temperatures. The calculation of FD is based on the definition of ETCCDI indices. Because of the regional distinction in extreme temperatures, SD and TN are calculated by the criterion given in Lee and Heo (2011) and Ha and Yun (2012). For example, according to the definition of Lee and Heo (2011), SD is identified as the annual number of days when Tmax is greater than 30°C. Based on the result of Ha and Yun (2012), TN is defined as the annual number of days on which daily Tmin is greater than 25°C. The extreme indices are categorized as either summer-based indices or winter-based indices. Summer-based indices are SD, TN, CDD, and GDD, while winter-based indices are FD and HDD. In other words, the daytime (nighttime) high temperature during summer can be represented by the SD (TN) while the FD is a representation

Table 1. The classification of subtropical climate zone used in this study. Here, T_{cold} and T_{warm} indicate the temperature of the coldest month and the warmest month, respectively. R_{smax} and R_{smin} indicate precipitation in the wettest month and the driest month during the summer, and R_{wmax} and R_{wmin} are same as R_{smax} and R_{smin}, but for the winter. Here, R_{wmin} and R_{smin} are less than 30mm.

Classification scheme	Climate zone	Definition
Trewartha (1968)	Subtropical Climate	$T_{cold} \le 18^{o}C$ and above 8 months with Tave $\ge 10^{o}C$
Köppen (1918)	Cwa (Humid subtropical climate with hot summer and dry winter)	$-3^{o}C \le T_{cold} < 18^{o}C$ and $T_{warm} \le 10^{o}C$ $R_{smax} \ge 10R_{wmin}$ $T_{warm} \ge 22^{o}C$
	Cfa (Humid subtropical climate with hot summer and year around precipitation)	$-3^{o}C \le T_{cold} < 18^{o}C$ and $T_{warm} \ge 10^{o}C$ Neither ($R_{smax} \ge 10R_{wmin}$) nor ($R_{wmax} \ge 3R_{smin}$) $T_{warm} \ge 22^{o}C$
	Dfa (Continental climate with hot summer and year around precipitation)	$T_{cold} < -3^{o}C$ and $T_{warm} \ge 10^{o}C$ Neither ($R_{smax} \ge 10R_{wmin}$) nor ($R_{wmax} \ge 3R_{smin}$) $T_{warm} \ge 22^{o}C$
	Dfb (Continental climate with warm summer and year around precipitation)	$T_{cold} < -3^{o}C$ and $T_{warm} \ge 10^{o}C$ Neither ($R_{smax} \ge 10R_{wmin}$) nor ($R_{wmax} \ge 3R_{smin}$) $T_{warm} < 22^{o}C$
	Dwa (Continental climate with hot summer and dry winter)	$T_{cold} < -3^{o}C$ and $T_{warm} \ge 10^{o}C$ $R_{smax} \ge 10R_{wmin}$ $T_{warm} \ge 22^{o}C$

Table 2. Definition of extreme indices used in this study.

Index	Definition
Summer Days (SD, unit: days)	annual number of days when Tmax ≥ 30°C
Tropical Nights (TN, unit: days)	The annual number of days Tmin ≥ 25°C
Frost Days (FD, unit: days)	The annual number of days when Tmin ≤ 0°C
Growing Degree Days (GDD, unit: °C)	The accumulated annual value by adding each day's 'Tave-T_{base}' when T_{base} = 10°C and Tave > T_{base}
Heating Degree Days (HDD, unit: °C)	The accumulated annual value by adding each day's 'T_{base}-Tave' when T_{base} = 18°C and Tave < T_{base}
Cooling Degree Days (CDD, unit: °C)	The accumulated annual value by adding each day's Tave-T_{base} when T_{base} = 24°C and Tave > T_{base}

of winter minimum. GDD is an index to relate plant and pest development rates, such as the date when a flower will bloom or a crop will reach maturity (Kim and Yun, 2008). HDD and CDD are widely used in the energy industry for calculation of consumption required to heat and cool buildings, respectively (Buyukakaca *et al*., 2001). Because the GDD, HDD, and CDD are values which accumulate annually, both temperature and the number of days when outside air temperatures are lower (or higher) than a specific base temperature (T_b) are important for determining the extreme indices. Note that base temperature has different values in the calculation of the different indices. Although the definition of the base temperatures for HDD and CDD differs from place to place, in East Asia, 18°C is generally considered as the base temperature for HDD and 24°C for CDD (Jiang *et al.*, 2009). In relation to GDD, the base temperatures of 0°C (brussel sprouts, cabbage), 5°C (peas, forages), and 10°C (corn, soybeans, tomatoes) are used for most agricultural crops (Gordan and Bootsma, 1993; Kim and Yun, 2008). Basically, 10°C is the most common base for GDD. Therefore, in this study, the base temperatures for GDD, HDD, and CDD are set at 10°C, 18°C, and 24°C, respectively. To represent the time series of the extreme indices, all indices are simply area-averaged over the Korean domain (34.2°-38.5°N, 126°-129.6°E). With focus on regional change over the Korean Peninsula, the area-average is only calculated for the land domain. For convenience, Tave is calculated by the average of Tmax and Tmin. The detailed definitions of these indices are summarized in Table 2.

3. Characteristics of extreme temperatures in the present climate

Changes in the subtropical climate zone and extreme climate indices are significantly related to daily Tmax and Tmin. In this section, we investigate the present characteristics of Tmax and Tmin over the Korean Peninsula. In addition, most models have a symmetric error in simulating the high frequency variability, due to internal noise. To validate the reliability of the model result, the simulated temporal and spatial patterns are compared with the observed patterns. The observation is an average of 76 station data, whereas the model is an average of land grid points over Korea. Figure 1 displays the annual cycle and probability density function (PDF) of daily Tmax and Tmin averaged over the Korean Peninsula during the annual period. Thus, the sample size is 25 (year) × 365 (day). Since Korea has a high degree of climatic seasonality with a large daily temperature range, a significant temperature range of about 30°C appears in the annual cycle (Figs. 1a and 1b). The warmest month is August, while the coldest month is January. The 20 km-AGCM reproduces well the annual cycle with the maximum in August and the minimum in January. Overall, the frequency distribution of daily temperature extremes exhibits two clear peaks (Figs. 1c and 1d). This is due to the evident seasonal temperature changes in the warmest month and the coldest month. The model underestimates the mean of Tmax (obs: 17.75 vs model: 15.66), while it overestimates the mean of Tmin (obs: 7.70 vs model: 8.88). However, the standard deviation is in good agreement with the observed variance (e.g., obs: 9.27 vs model: 9.15 in Tmax). Note that the threshold indices are highly dependent on mean bias of simulated absolute value. This suggests the necessity of bias correction in model. To gain a reliable result, we have carried out the bias correction using a moment adjustment. The correction is performed using the daily Tmax and Tmin area-averaged for all land grids over Korea. Since the second moment (i.e., standard deviation) in model nearly corresponds with that in observation, the first moment (i.e., mean) is only adjusted in model. Thus, the mean bias correction is given by the monthly difference between the model mean and the observation mean, considering the change in seasonal cycle. In detail, these simulated daily extreme temperatures are corrected by subtracting the difference between the monthly means in model and observation, respectively. The monthly mean biases made by area-averaged extreme temperatures are also applied as a same correction factor for every grid to calculate the bias-corrected spatial distribution of extreme temperatures. The bias-corrected PDF is represented in Figs. 1e and 1f. The simulated bias-correction distribution reasonably captures the probability of the observed daily temperature occurrence and the temperature range. Tmax reveals a more asymmetric double-peak distribution than Tmin, which is reasonably represented in the simulation. Consequently, the model reproduces well the observed annual cycle and prob-

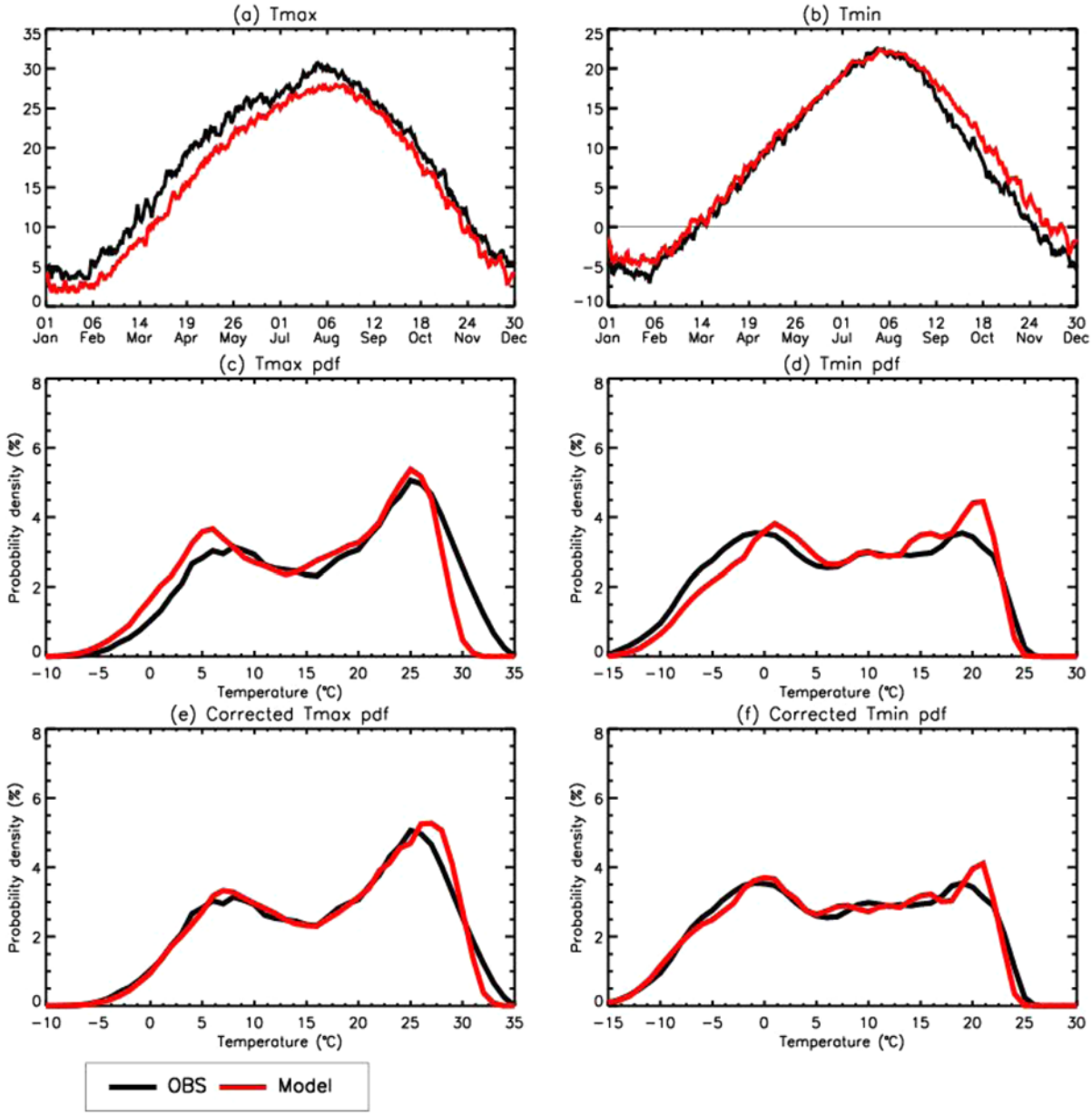

Fig. 1. The annual cycle of observed and simulated daily (a) maximum temperature and (b) minimum temperature, and probability density function of daily (c) maximum temperature and (d) minimum temperature. (e) and (f): same as Figs. (c) and (d), but for the bias-corrected (e) maximum temperature and (f) minimum temperature.

ability of extreme temperature occurrence. Hereafter, the model results are suggested by the mean bias-corrected temperatures.

The change in extreme climate indices is strongly related to Tmax and Tmin in the warmest month and coldest month. The spatial distribution of Tmax in August and Tmin in January is shown in Fig. 2. There are some differences in spatial characteristics of the observed and simulated temperatures. For example, the model somewhat overestimates the extreme temperatures (especially Tmax) over the Sobaek mountain chain and the northwestern part of this mountain chain (see Fig. 3a for topography), while underestimates the temperatures over the southeastern coast region of the Korean Peninsula. In addition, the minimum of Tmin over the Taebaek Mountains is overestimated in model. Although the maximum (or minimum) position and intensity in model are slightly different from those in observation, the observed spatial characteristics are realistically simulated by the model. Tmax is higher in the southern and western part of the Korean Peninsula and lower in the northeastern part (i.e., the high mountain region). The difference in spatial pattern is caused by topographical effects (the Taebaek Mountains is in the northeastern part and the Sobaek mountain chain stretches southwestward from Taebaek). On the other hand, Tmin exhibits slightly different features from Tmax: Tmin exhibits a maximum in the southern coast region;

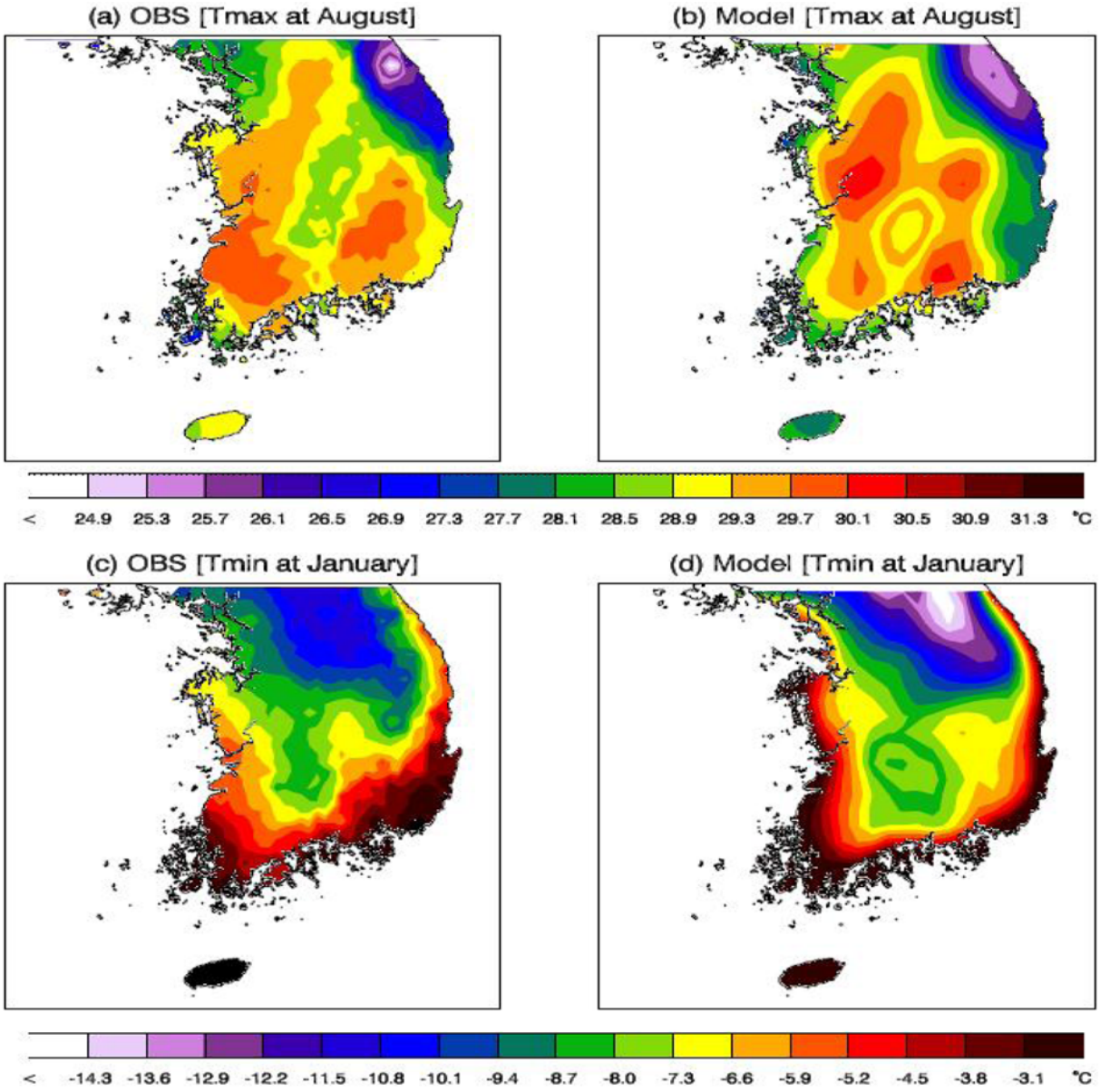

Fig. 2. The spatial distribution of the (a) observed and (b) simulated daily maximum temperature in August during 1979-2003, and the (c) observed and (d) simulated daily minimum temperature in January during 1979-2003.

Tmax shows a relatively large value in the northwestern part compared to Tmin. The asymmetry between Tmin and Tmax has been reported in many previous studies (e.g., Karl *et al.*, 1991; Im *et al.*, 2011). The asymmetry of extreme temperatures in time and space could contribute to the different changes in extreme climate events associated with Tmax and Tmin. In the next section, we will investigate future changes in the subtropical climate zone and extreme climate indices.

4. Changes in the future climate

Under a global warming climate, accurate projection of future climate contributes to the exact assessment of climate change impact, and to the development of adaptation strategies for possible climate changes. In this section, the future changes in the subtropical climate zone and extreme climate indices are quantitatively analyzed. To calculate the subtropical climate zone and extreme climate indices, the mean bias-corrected temperatures suggested in Section 3 are used.

To examine the change in the subtropical climate zone, the Trewartha and Köppen schemes are applied. Figure 3a displays the spatial change of the subtropical climate zone based on the Trewartha definition in the present, near-future, and future climates. In the present climate, the simulated subtropical region is restricted to the southern coast including Jeju Island and Mokpo, corresponding to the observed results in Kwon *et al.* (2007). In the near-future climate, the subtropical region moves slightly northward. In the future climate, the subtropical climate

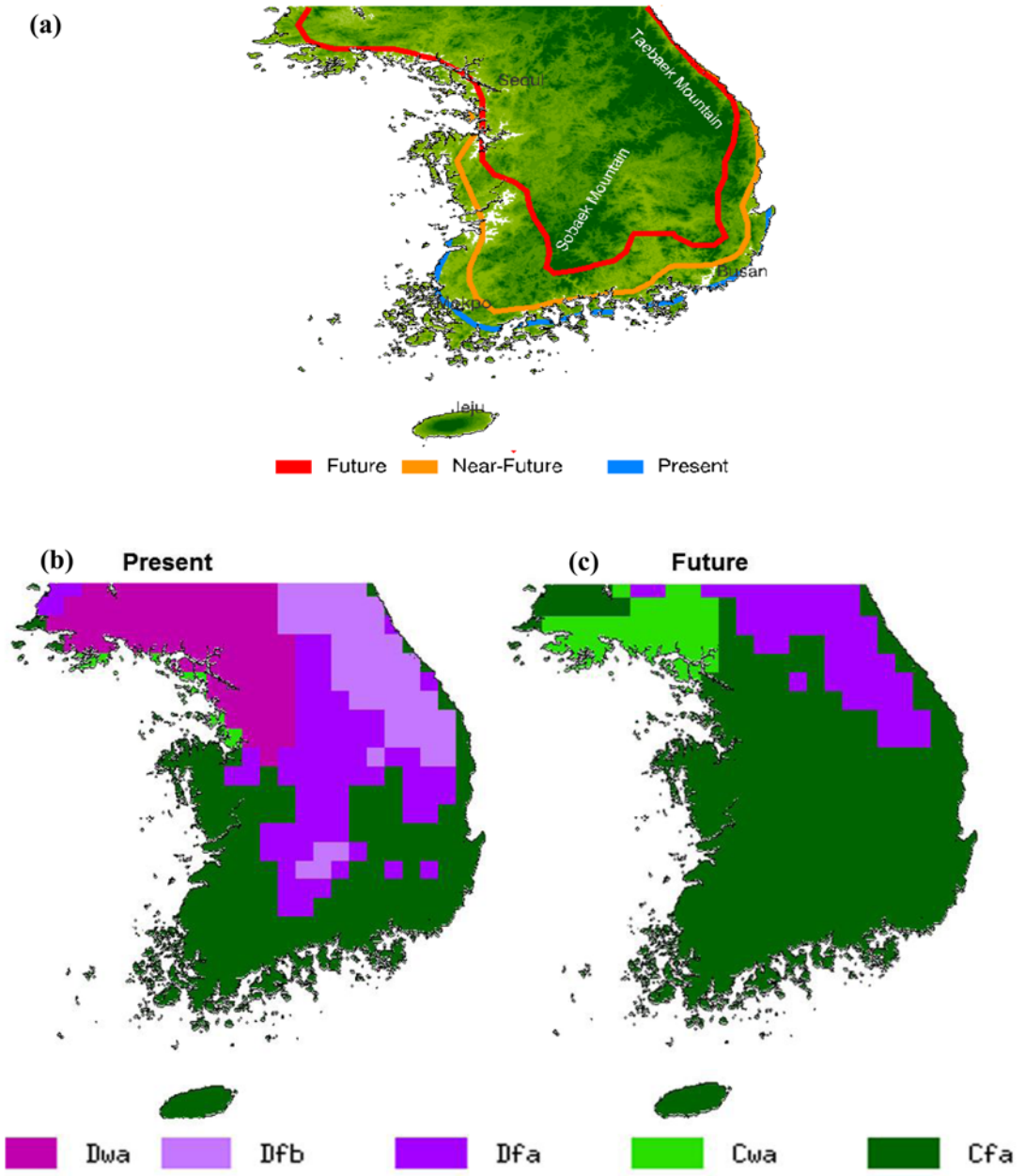

(d)	Cwa	Cfa	Dwa	Dfa	Dfb
Present	1.1%	41.9%	20.0%	21.7%	15.4%
Future	8.7%	76.9%	0.0%	14.5%	0.0%

Fig. 3. (a) Changes in the subtropical climate zone based on the Trewartha climate classification. The subtropical climate zone based on the Köppen climate classification in the (b) present-day and (c) future climate (2075-2099). (d) The ratio of Köppen climate classification zones in the present and future climate.

region moves further northward and covers many southwestern coastal regions. Overall, the northward shift of the subtropical climate region is consistent with topographical features including the Taebaek and Sobaek mountain chains. Due to topographical effects, the change is more pronounced in the western part of the Korean Peninsula than in the eastern part. The percentage of the total climatic regime composed of subtropical climate zone increases from present to future climate, with

present, near-future, and future subtropical climate zones making up 7.8%, 13.5%, and 28.8% of total climate region, respectively. This suggests a future increase in subtropical climate zone of about 21% based on the Trewartha scheme.

The climate classification based on the Köppen scheme reveals a more pronounced change in the subtropical climate region (Figs. 3b and 3c). In the present climate, there are climate regions of Cwa, Cfa, Dwa, Dfa, and Dfb. Year-round humid and warm temperate climate (Cfa), which corresponds to the subtropical climate zone, appears on the southern part of the Korean Peninsula except for the Sobaek mountain region. The northern part consists mainly of Dwa, Dfa, and Dfb (continental/microthermal climate). The Sobaek and Taebaek mountain regions exhibit Df with a year-round humid and subarctic climate. On the western side of the Taebaek region, a subarctic climate with heavy rainfall in summer and dryness in winter (Dwa) appears. In the future climate, except for the northern part of the Korean Peninsula and the Taebaek maintain region, Cfa corresponding to the subtropical climate zone is shown in most of the Korean Peninsula, due to a warmer future climate. The percentages of climate classifications under the present and future climates are presented in Fig. 3d. The Cfa region increases by 35%, while the Dwa and Dfb zones both decrease by about 20%. Although the delineation of the subtropical climate region is slightly different between the Trewartha and Köppen classifications, the climate classification produces a coherent change in climate region, in terms of topographical effects. The increase of the subtropical climate region is reasonably consistent with future rainfall change with a longer rainy season (e.g., Yun *et al.*, 2008). This may suggest greater extreme climate events including heavy rainfall, extreme climates, and consequently, damage from natural disasters in

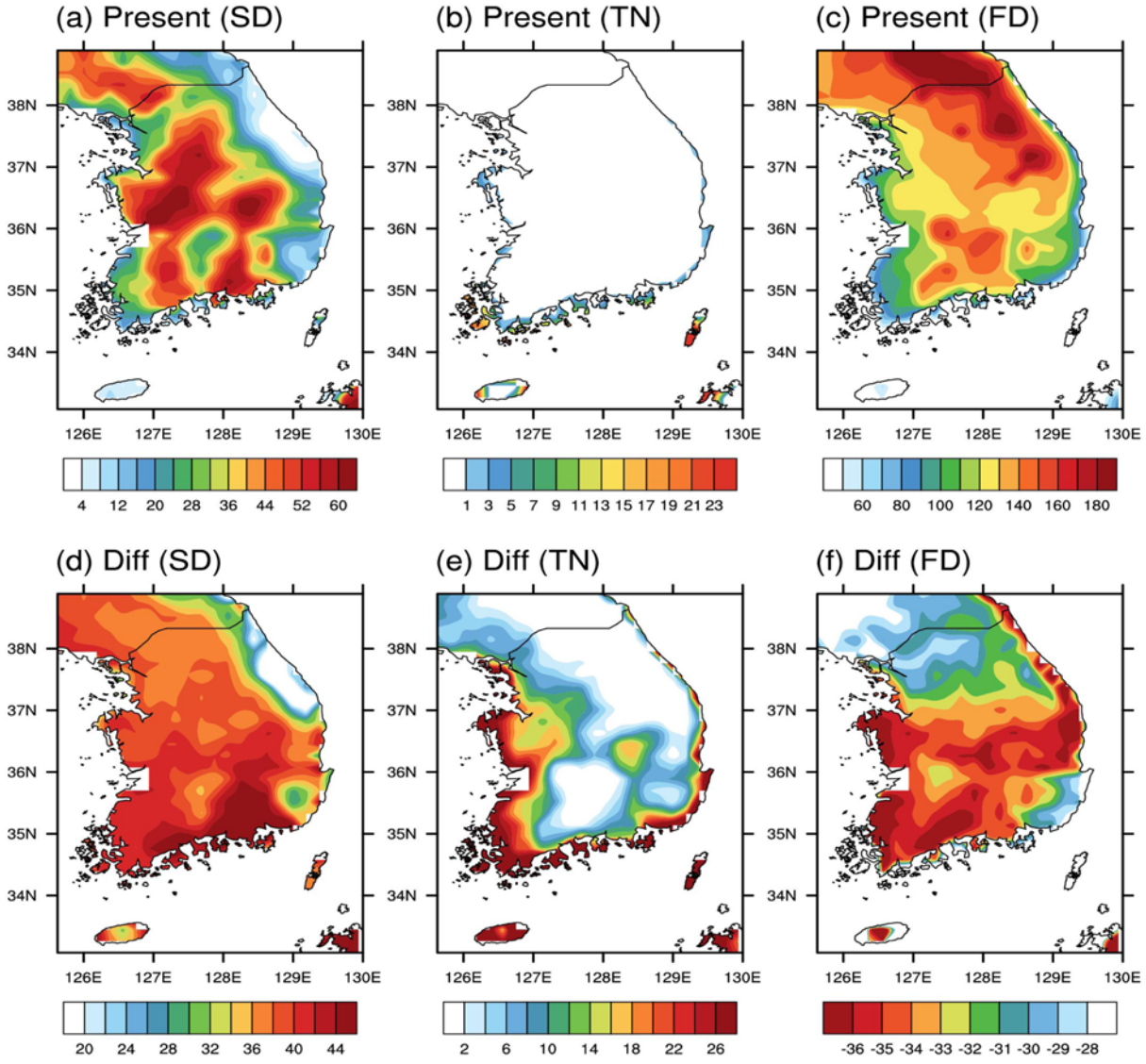

Fig. 4. Spatial patterns of (a) SD, (b) TN, (c) FD during the present climate. The difference between the present-day and future climate (2075-2099) for (d) SD, (e) TN, and (f) FD.

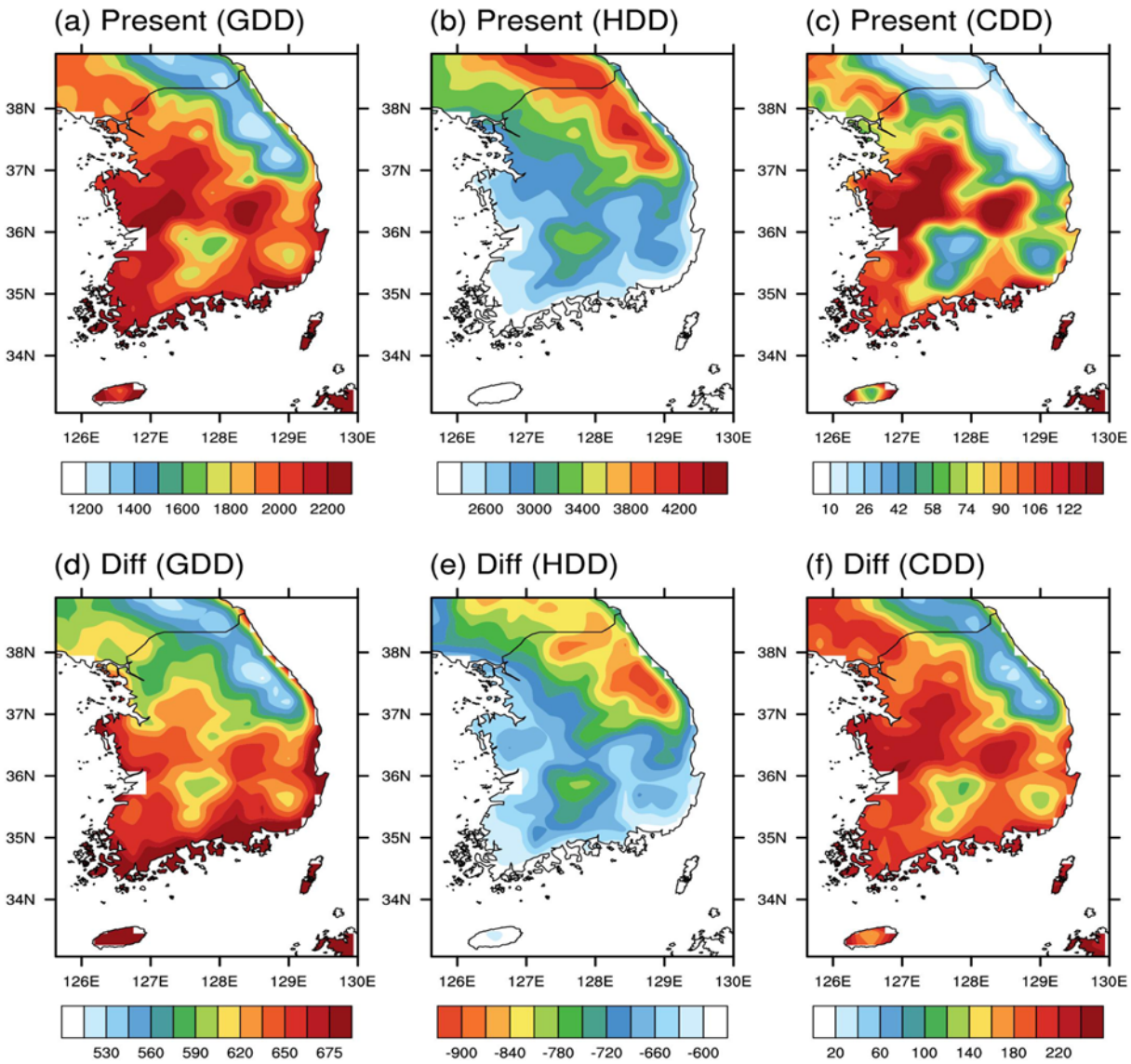

Fig. 5. Same as Fig. 4, but for GDD, HDD, and CDD.

coastal region.

With the change in the subtropical climate zone, we investigate the future change in extreme climate indices. Figures 4 and 5 display the spatial patterns of SD, TN, FD, GDD, HDD, and CDD in the present climate and the difference between the present and future climate. Only differences from the future climate (from 2075 to 2099) are studied. In Fig. 4a, the present SD distribution reveals widely separated geographical centers except for in the Taebaek mountain chain. The high values appear mainly inland rather than in the coastal regions. The SD field resembles the Tmax distribution in Fig. 2b. In the future projection, SD values are largely increased in most regions. The increase is particularly evident in the southern and western part of the Korean Peninsula. It should be noted that the difference in Fig. 4d is analogous to the present structure, implying that regions with a higher SD in the present climate tend to experience a larger increase in SD.

In contrast to SD, TN in the present climate occurs in the narrow southern and western coastal region (Fig. 4b). The remarkable difference between SD and TN is that a larger TN is for coastal regions, but a larger SD in inland regions. This may be partially caused by the fact that SD is related to the day-time temperature (Tmax) in warmer inland temperatures, while TN is associated with the nighttime temperature (Tmin) in warmer coastal temperatures. The thermal difference is due to thermal inertia between land and ocean. The difference from the future climate also indicates a greater increase in the southern and western coastal regions, while the mountain regions do not exhibit any evident change (Fig. 4e). The most notable future change follows the present structure of TN.

The spatial structure of FD is opposite to that of TN (Fig. 4c), because FD is related to the lower-tail distribution of

Tmin, while TN is link to the upper-tail distribution of Tmin (see Fig. 1d). Thus, in relation to Tmin structure (Figs. 2c and 2d), the two indices of TN and FD have a similar spatial structure but opposite phase. The spatial distribution in FD is negatively associated with the Tmin distribution. FD in the future climate decreases by about 30-40 days over the entire domain of Korea. Note that the future difference in FD is slightly different from the present structure. The difference is in part similar to the future change in TN. A large decrease in FD appears in the western coastal region. There are large decreases along the southern part of high-altitude regions in the Taebaek and Sobaek Mountains. These changes may be related to a warmer Tmin structure during winter.

In relation to the degree days, GDD and CDD are summer-based indices, while HDD is winter-based index. The spatial structures in the present climate exhibit a signal consistent with those of Tmax and Tmin (Fig. 5). Thus, GDD and CDD show a similar spatial pattern, while HDD reveals the opposite spatial structure. As shown in Figs. 5d and 5f, the future change in GDD, HDD, and CDD follows the horizontal structure in the present climate. GDD and CDD exhibit a larger increase in the southern and western coastal region, while HDD shows a larger decrease in the high-altitude regions of the Taebaek and Sobaek Mountains. Consequently, the spatial pattern of extreme indices is significantly related to the geographical distribution of Tmax and Tmin associated with the indices. The future changes in extreme indices are roughly contributed to the present structure of extreme indices in relation to land-ocean thermal inertia and topographical effect.

To understand the increasing or decreasing trends of regionally averaged indices, the interannual variability of regionally averaged extreme indices over the Korean Peninsula is shown in Fig. 6. The broken section of the time series is caused by time-splice global warming projection of the high resolution model. Among the six extreme temperature indices, SD, TN, GDD and CDD show an increasing trend, while FD and HDD are in decreasing trend. The increasing or decreasing slopes are significant in all extreme indices. To compare the change quantitatively, percentage change is summarized in Fig. 7. The change of extreme indices between the present and near-future climate is relatively small and the ratio of change accelerates abruptly in the future climate. Overall, SD, TN, and CDD

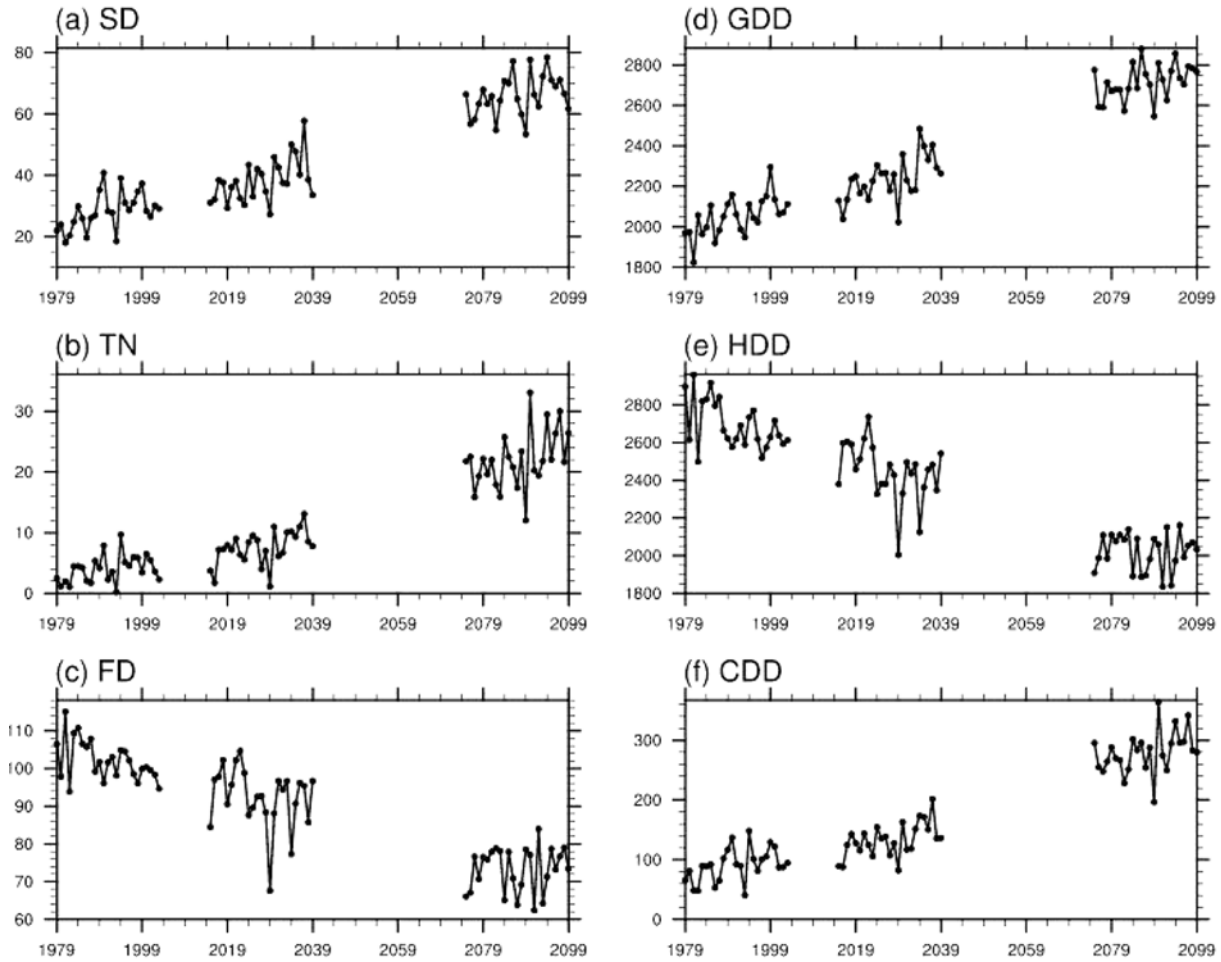

Fig. 6. Temporal variation of regionally averaged indices of (a) SD, (b) TN, (c) FD, (d) GDD, (e) HDD and (f) CDD over the Korean Peninsula from 1979 to 2099, based on model integration period of present (1979-2003), near future (2015-2039) and future (2075-2099).

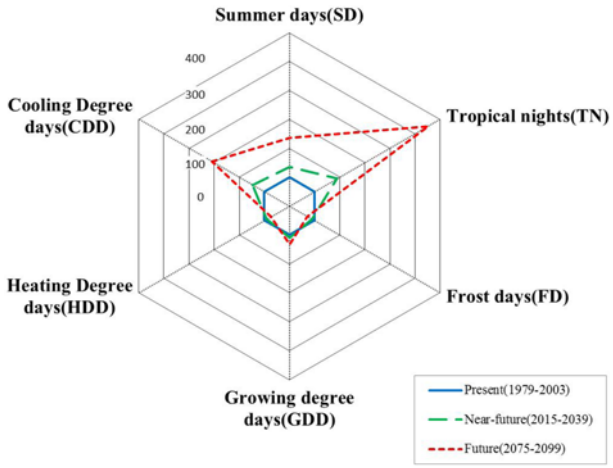

Fig. 7. Summary of change rates in the extreme climate indices (unit: %).

exhibit a prominent change in the future climate, while HDD, GDD, and FD show relatively little change. The most significant increase is seen in TN (+452%) and the most significant decrease is appeared in HDD (−25%). The summer-based indices such as SD, TN, and CDD exhibit a larger percentage change than the winter-based indices such as HDD and FD. This agrees well with the model results of Ho *et al.* (2011), using the National Center for Atmospheric Research (NCAR) Community Climate System Model 3 (CCSM3). A larger percentage change reflects a greater contribution of summer-based extreme events in the warmer future climate.

Notice that the ratio of future change is larger for CDD than for HDD. The larger change ratio of CDD has an important implication for energy requirements in the future climate. Why is the future change larger for CDD than for HDD? To answer the question, we compare the future change between HDD and CDD in terms of day frequency and temperature change, represented in Table 3. Here, HDD and CDD are good indices to illustrate the effect on both frequency and intensity of the extreme temperature events. As shown in Fig. 7, the change ratio of HDD (a decrease of 25%) is much smaller than that of CDD (an increase of 209%). Despite the low change of HDD, the temperature averaged during the selected HDD reveals a slightly larger future change than that averaged during the CDD. Conversely, the accumulated number of days in CDD is significantly larger than that in HDD. Consequently, the increasing frequency induces a greater change ratio in CDD. On the other hand, unlike the change ratio, the decrease in HDD absolute value (~673) is much larger than the increase in CDD (~189), due to a higher annual frequency of day number in HDD (e.g., 233 in the present HDD but 48 in CDD). The significant change in absolute value will be important for climate adaptation of energy sector, as well.

Why does the change in CDD reveal a larger frequency regardless of a lower temperature? To understand the changes in mean and frequency related to CDD and HDD, we investigate the PDF of daily Tave, Tmax, and Tmin during

Table 3. The indictors of HDD and CDD in the present and future climate (2075-2099).

Indices	Indicator (unit)	Present	Future
HDD	HDD (°C)	2693.16	2020.27
	Change of HDD (%)	0	-25.0
	Day number (day) : a	233	199
	Temp per day (°C day^{-1}) : b	11.34	9.87
	Change of a/b		**1.47**/34
CDD	CDD (°C)	90.73	280.01
	Change of CDD (%)	0	+280.6
	Day number (day) : a	48	89
	Temp per day (°C day^{-1}) : b	1.66	3.02
	Change of a/b		1.36/**41**

January and August (i.e., the coldest month and warmest month), respectively (Fig. 8). The sample size is 775 (31 days × 25 years). During January, the change in Tave between future and present climate is 3.24°C (−0.68°C to 2.56°C), while that during August is 2.91°C (25.23°C to 28.14°C). The change during January is larger than that during August. The greater temperature change in HDD can be understood by a larger temperature change in January than in August. Looking into the detailed change in terms of Tmax and Tmin, during January, the change in Tmax is 3.05°C (4.13°C to 7.18°C), while that during August is 2.74°C (29.22°C to 31.96°C). The change in Tmin during January is 3.42°C (−5.48°C to −2.06°C), while that during August is 3.09°C (21.24°C to 24.33°C). Tmin reveals a larger increase rather than Tmax during January and August. The asymmetric response of Tmax and Tmin due to global warming is reasonably consistent with the globally observed evidence suggested by the previous studies (Karl *et al.*, 1991; Easterling *et al.*, 1997).

The more frequent changes of CDD may be due to the different distribution of extreme temperatures between winter and summer. As shown in Fig. 8, the frequency distribution during January is lower and broader, while that during August is higher and narrower. The frequency distribution during January has about 3 standard deviations, whereas that during August has almost 1.5. The concentrated frequency probability during the summer season can have a more significant effect on increasing the frequency of extreme indices during the summer season. Therefore, although the future change of HDD has a greater intensity than that of CDD, more frequent occurrences of CDD lead to a larger increase of change ratio in the future climate.

5. Conclusion and discussion

In the present study, we investigate the future changes in the subtropical climate zone and six extreme indices, using the 20-km high-resolution AGCM. For this purpose, the climates for the periods present, near future, and future climate correspond-

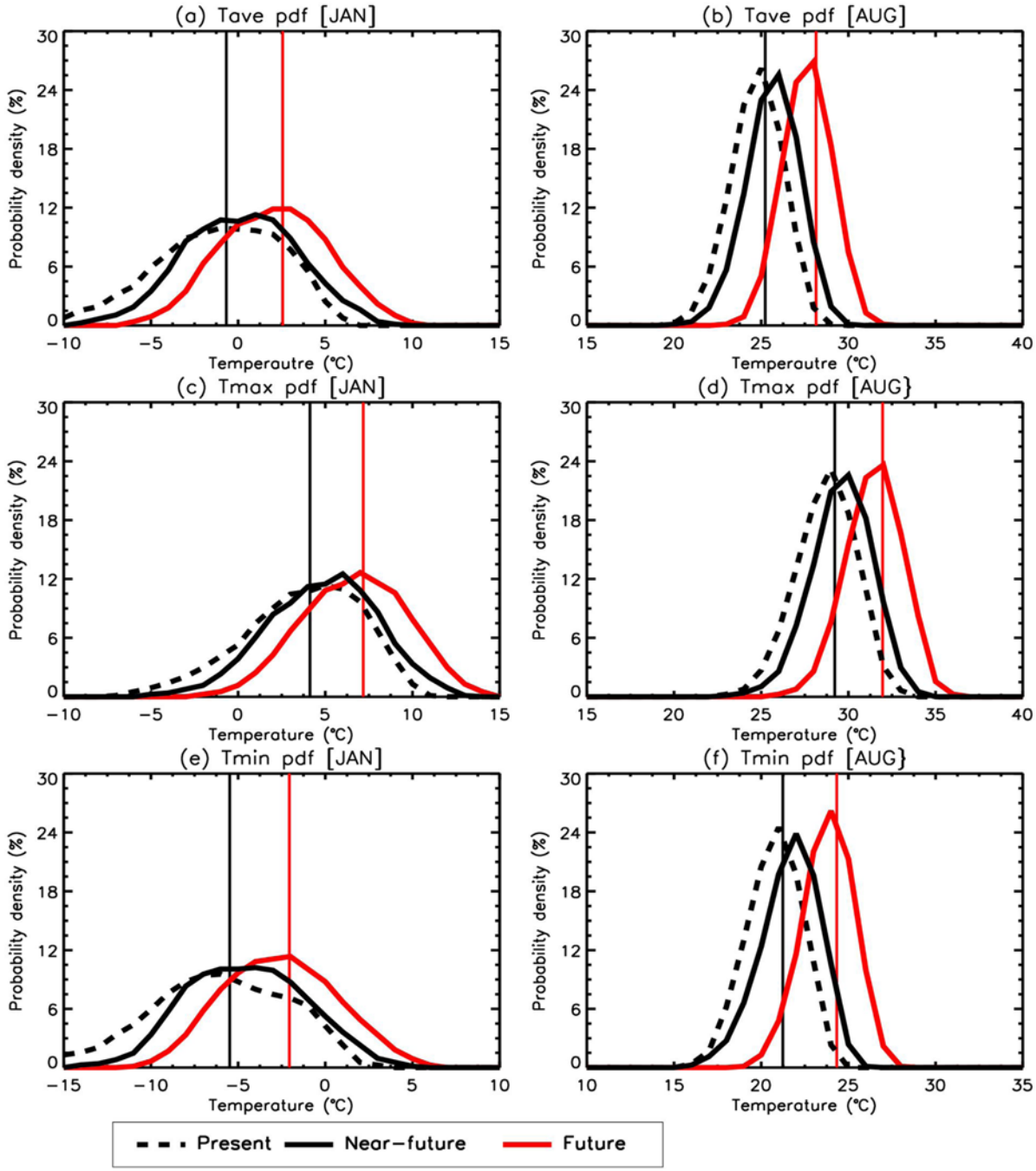

Fig. 8. Probability density functions of daily (a) mean temperature, (c) maximum temperature, and (e) minimum temperature during the January period and of daily (b) mean temperature, (d) maximum temperature, and (f) minimum temperature during the August period. The perpendicular black and red lines indicate the mean in the present and future climate (2075-2099), respectively.

ing to 1979-2003, 2015-2039 and 2075-2099, respectively, are considered. In relation to the subtropical climate zone and extreme indices, the two climate classification schemes of Trewartha (1968) and Köppen (1918) are applied. Four summer-based indices (i.e., summer days, tropical nights, growing degree days, and cooling degree days) and two winter-based indices (frost days and heating degree days) are used. To gain a reliable result, the mean bias in model is corrected by the monthly difference between the model mean and the observation mean, considering the change in seasonal cycle. The model reasonably reproduces the annual cycle of daily Tmax and Tmin with the maximum in August and the minimum in January, and the frequency probability of extreme temperature occurrence over Korea. In addition, the model simulates well the spatial distribution of extreme temperatures associated with topography. This provides reliability in assess-

ments of regional changes in extreme climate events over Korea.

In the future climate, the subtropical climate zone moves gradually northward. Overall, due to topographical effects, the northward shift of the subtropical climate region is more evident in the southwestern coastal regions than inland and mountain regions. According to the Trewartha scheme and Köppen scheme, the subtropical climate zone increases by 21% and 35%, respectively. The increased subtropical climate zone suggests a greater possibility of extreme climate events such as heavy rainfall, and consequently, damage caused by natural disasters in coastal regions. The spatial change in extreme climate indices follows the geographical characteristics in terms of land-ocean thermal inertia and topographical effects. Therefore, regions with higher extreme indices in the present climate tend to exhibit a larger increase. In a consistent response with the changes in the subtropical climate zone, the change is manifested more in coastal regions than in inland regions, except for the change in SD and HDD. Consequently, the summer-based indices such as SD, TN, GDD and CDD exhibit an increasing trend, while the winter-based indices such as FD and HDD show a decreasing trend. The most significant increase is presented in TN (+452%) and the smallest change is shown in HDD (–25%). The summer-based indices such as SD, TN, and CDD exhibit a larger percentage change than the winter-based indices such as HDD and FD.

As an important implication of the change in extreme events, HDD and CDD, which are vital indicators of energy-saving applications, are examined with respect to changes in frequency and intensity. The future change in CDD displays a higher frequency but a lower temperature than that in HDD. Eventually, the increasing frequency results in a greater increase of change ratio in CDD. Unlike the change ratio, the change in absolute value reveals a larger change in HDD than in CDD. The different change aspects could be considered for the climate adaptation of energy sector. The more frequent changes of CDD may be due to a higher and less dispersed occurrence probability of extreme temperatures during the summer season. The greater increase in extreme climate events, regardless of the lower temperature change, remains important factors in prediction of the future change in extreme climate events. In addition, the different seasonal change introduces a requirement for different seasonal assessments of the change in extreme climate events.

On the other hand, Li *et al.* (2009) have shown that the observed summertime variability of climate extreme temperatures in Korea is consistent with that over northern China, while the wintertime variability in Korea is similar to that over eastern China. This study for the future change in extreme climate events may contribute improvements to the assessment of climate change impacts over Korea and, by extension, over East Asia. Therefore, the quantitative interpretation and analysis of future changes in extreme climate events will provide useful information to prevent future damages to the social infrastructure due to global warming. Although the increase in mean temperature is associated with an increase in the frequency and intensity of extreme climate events, the change in extreme climate events may be controlled by more complex dynamics (e.g., different modulating factors, intra-seasonal variability, and solar cycle change). To understand the problem of extreme climate change, more detailed investigation is necessary in the future study.

Acknowledgements. This GRL work was supported by the National Research Foundation of Korea (NRF) grant funded by the Korea government (MEST) (No. 2011-0021927) in Korea and by the KAKUSHIN program funded by the Ministry of Education, Culture, Sports, Science and Technology (MEXT) in Japan. The calculations were performed on the Earth Simulator in Japan.

REFERENCES

Alexander, L. V., and J. M. Arblaster, 2008: Assessing trends in observed and modelled climate extremes over Australia in relation to future projections. *Int. J. Climatol*., **29**, 417-435.

_____, and Coauthors, 2006: Global observed changes in daily climate extremes of temperature and precipitation. *J. Geophy. Res*., **111**, D05109, doi:10.1029/2005JD006290.

Bonsal, B. R., X. Zhang, L. A. Vincent, and W. D. Hogg, 2001: Characteristics of daily and extreme temperatures over Canada. *J. Climate*, **14**, 1959-1976.

Boo, K.-O., W.-T. Kwon, and H.-J. Baek, 2006: Change of extreme events of temperature and precipitation over Korea using regional projection of future climate change. *Geophy. Res. Lett*., **33**, L01701, doi:10.1029/2005GL023378.

Buyukalaca, O., H. Bulut, and T. Yilmaz, 2001: Analysis of variable-base heating and cooling degree-days for Turkey. *Applied Energy*, **69**, 269-283.

Easterling, D. R., B. Horton, P. D. Jones, T. C. Peterson, T. R. Karl, and D. E. Parker, 1997: Maximum and minimum temperature trends for the globe. *Science*, **277**, 364-367.

Feng, L., T. Zhou, B. Wu, T. Li, and J.-J. Luo, 2011: Projection of future precipitation change over China with a high-resolution global atmospheric model. *Adv. Atmos. Sci.*, **28**(2), 464-476, doi: 10.1007/s00376-010-1016-x.

Gordon, R., and A. Bootsma, 1993: Analyses of growing degree-days for agriculture Atlantic Canada. *Climate Res.*, **3**, 169-176.

Ha, K.-J., and K.-S. Yun, 2012: Climate change effects on tropical night days in Seoul, Korea. *Theor. Appl. Climatol.*, **109**, 191-203, doi:10.1007/s00704-011-0573-y.

Ho, C.-H., and Coauthors, 2011: A projection of extreme climate events in the 21st century over East Asia using the community climate system model 3. *Asia-Pacific J. Atmos. Sci.*, **47**(4), 329-344.

Im, E.-S., I.-W. Jung, and D.-H. Bae, 2011: The temporal and spatial structures of recent and future trends in extreme indices over Korea from a regional climate projection. *Int. J. Climatol*., **31**, 72-86.

Jiang, F., X. Li, B. Wei, R. Hu, Z. Li, 2009: Observed trends of heating and cooling degree-days in Xinjiang Province, China. *Theor. Appl. Climatol.*, **97**, 349-360.

Jung, I.-W., D.-H. Bae, and G. Kim, 2011: Recent trends of mean and extreme precipitation in Korea. *Int. J. Climatol*., **31**, 359-370.

Karl, T. R., G. Kukla, V. N. Razuvayev, M. J. Changery, R. G. Quayle, R. R. Heim Jr., D. R. Easterling, and C. B. Fu, 1991: Global warming: Evidence for asymmetric diurnal temperature change. *Geophys. Res. Lett.* **18**, 2253-2256.

Kharin, V. V., F. Zwiers, X. Zhang, and G. C. Hegerl, 2007: Changes in temperature and precipitation extremes in the IPCC Ensemble of Global Coupled Model Simulations. *J. Climate*, **20**, 1419-1444.

Kiktev, D., J. Caesar, L. V. Alexander, H. Shiogama, and M. Collier, 2007: Comparison of observed and multimodeled trends in annual extremes of temperature and precipitation. *Geophy. Res. Lett*., **34**, L10702, doi: 10.1029/2007GL029539.

Kim, J.-H., and J. I. Yun, 2008: On mapping growing degree-days (GDD) from monthly digital climate surfaces for South Korea, *Korean J. of Agri. and Fore. Meteorol*., **10**(1), 1-8 (in Korean with English abstract).

Kitoh, A., and S. Kusunoki, 2008: East Asian summer simulation by a 20-km mesh AGCM. *Climate Dyn.*, **31**, 389-401.

Köppen, W. P., 1918: Klassification der Klimate nach Temperatur, Niederschlag und Jahreslauf. *Petermanns Geogr. Mitt.*, **64**, 193-203.

Kwon, Y.-A., W.-T. Kwon, K.-O. Boo, Y. Choi., 2007: Future Projections on Subtropical Climate Regions over South Korea Using SRES A1B Data. *Journal of the Korean Geographical Society*, **42**(3), 355-367 (in Korean with English abstract).

Lee, S., and I. Heo, 2011: The impacts of urbanization on changes of extreme events of air temperature in South Korea. *J. of Korean Geog. Soc*., **46**(3), 257-276 (in Korean with English abstract).

Li, H., L. Feng, and T. Zhou, 2011a: Multi-model Projection of July-August Climate Extreme Changes over China under CO2 Doubling. Part I: Precipitation, *Adv. Atmos. Sci.*, **28**(2), 433-447,doi:10.1007/s00376-010-0013-4.

_____, _____, and _____, 2011b: Multi-model Projection of July-August Climate Extreme Changes over China under CO2 Doubling. Part II: Temperature, *Adv. Atmos. Sci.*, **28**(2), 448-463,doi:10.1007/s00376-010-0052-x.

_____, T. Zhou, and J.-C. Nam, 2009: Comparison of daily extreme temperatures over eastern China and South Korea between 1996-2005. *Adv. Atmos. Sci.*, **26**(2), 253-264, doi:10.1007/s00376-009-0253-3.

Meehl, G. A., and Coauthors, 2000: An introduction to trends in extreme weather and climate events: Observations, socioeconomic impacts, terrestrial ecological impacts, and model projection: *Bull. Amer. Meteor. Soc.*, **81**, 413-416.

Mizuta, R., Y. Adachi, S. Yukimoto, S. Kusunoki, 2008: Estimation of future distribution of sea surface temperature and sea ice using CMIP3 multi-model ensemble mean. *Technical Report of Meteorological Research Institute*, **56**, 28 pp.

Rolim, G. S., M. B. P. Camargo, D. G. Lania, and J. F. L. Moraes, 2007: Climatic classification of Köppen and Thornthwaite sistems and their applicability in the determination of agroclimatic zonning for the state of São Paulo, Brazil. *Bragantia*, **66**(4), 711-720.

Trenberth, K.E., and Coauthors, 2007: Observations: surface and atmospheric climate change. In: *Climate Change 2007: The Physical Science Basis. Contribution of Working Group I to the Fourth Assessment Report of the Intergovernmental Panel on Climate Change*, Solomon, S., and Coauthors, Eds., Cambridge University Press, Cambridge, United Kingdom and New York, NY, USA.

Trewartha, G. T., 1968: An Introduction to weather and Climate. 4th edition, McGraw-Hill, New York, 408 pp.

Yun, K.-S., S.-H. Shin, K.-J. Ha, A. Kitoh, and S. Kusunoki, 2008: East Asian Precipitation Change in the Global Warming Climate simulated by a 20-km mesh AGCM. *Asia-Pacific J. Atmos. Sci.*, **44**(3), 233-247.

Zhai, P., X. Zhang, H. Wan, and X. Pan, 2005: Trends in total precipitation and frequency of daily precipitation extremes over China. *J. Climate*, **18**, 1096-1108.